Theoretical and experimental (*e*,2*e*) study of electron-impact ionization of laser-aligned Mg atoms

Sadek Amami,[1] Andrew Murray,[2] Al Stauffer,[3] Kate Nixon,[2,*] Gregory Armstrong,[4] James Colgan,[4] and Don Madison[1]

[1]*Physics Department, Missouri University of Science and Technology, Rolla, Missouri 65409, USA*
[2]*Photon Science Institute, School of Physics and Astronomy, University of Manchester, Manchester M13 9PL, United Kingdom*
[3]*Department of Physics and Astronomy, York University, Toronto, Ontario, Canada M3J 1P3*
[4]*Theoretical Division, Los Alamos National Laboratory, Los Alamos, New Mexico 87545, USA*

We have performed calculations of the fully differential cross sections for electron-impact ionization of magnesium atoms. Three theoretical approximations, the time-dependent close coupling, the three-body distorted wave, and the distorted wave Born approximation, are compared with experiment in this article. Results will be shown for ionization of the 3*s* ground state of Mg for both asymmetric and symmetric coplanar geometries. Results will also be shown for ionization of the 3*p* state which has been excited by a linearly polarized laser which produces a charge cloud aligned perpendicular to the laser beam direction and parallel to the linear polarization. Theoretical and experimental results will be compared for several different alignment angles, both in the scattering plane as well as in the plane perpendicular to the incident beam direction.

I. INTRODUCTION

One of the recent significant advances in the field of electron-impact ionization of molecules, or (*e*,2*e*), has been the development of the capability to measure ionization of aligned molecules [1–5] which provides a more sensitive test of theory than measurements which average over all molecular alignments [6–10]. On the atomic level, the equivalent measurement would be ionization of atoms that have been excited by a linearly polarized laser which produces a charge cloud aligned with the polarization axis of the laser beam. Nixon and Murray [11,12] have performed such a measurement for laser-aligned Mg, and the purpose of this work is to see how well our theoretical calculations compare with the measurements.

Measurements were made for ionization of both the ground 3*s* state as well as the laser-aligned 3*p* state, and all measurements were symmetric for final-state energies (i.e., $E_1 = E_2$). For the 3*s* state, both symmetric and asymmetric angles were examined while for the 3*p* state only asymmetric angular geometries were measured. For the aligned 3*p* state, two different measurements were performed—atomic alignment in the perpendicular plane (the plane perpendicular to the beam direction and perpendicular to the scattering plane) [11] and atomic alignment in the scattering plane [12]. In total, nine different angular distributions were measured for nine different alignment directions. However, Stauffer [13] showed that all of these nine different angular distributions (or as many more as you want) can be obtained from the $m = (0,1)$ amplitudes calculated relative to the incident beam direction.

II. THEORY

We have used both the perturbative three-body distorted wave (3DW) approach and the nonperturbative time-dependent close coupling (TDCC) approach to describe the process of interest. Each of them has been described

previously. Hence we will only summarize them briefly to the extent necessary for the present discussion, with references where interested readers can find more information.

A. TDCC

The TDCC calculations presented here have been discussed in detail previously [14]. The TDCC method centers around the propagation of a two-electron wave function that accounts for the interaction between the incoming electron and the ionized electron of the target. The interaction of this two-electron wave function with the remaining electrons is included through direct and local exchange potentials. The calculations presented here for electron-impact ionization of ground-state Mg ($3s^2$) were found to require a large number of coupled channels to converge, and required inclusion of partial waves from $L = 0$ to 12. TDCC calculations for two active electrons are also possible for ionization of excited-state Mg ($3s3p$). However, such calculations only describe the initial state as a ($3s3p$) configuration, whereas the measurements of interest [11,12] probe ionization from the $3s3p\ ^1P$ term. Within a three-electron TDCC approach [15], one may construct a three-electron wave function that properly accounts for the spin symmetry of the initial $3s3p\ ^1P$ term. However, such calculations are very computationally demanding and are difficult to run to convergence, and so will not be presented here.

B. 3DW

The three-body distorted wave (3DW) approach has been fully described in previous works [16,17]. As usual, we evaluate both the direct and exchange amplitudes. For the case of the laser-aligned 3*p* state, the *T* matrix will depend on the orientation of the initial-state wave function $\Phi_i(\hat{\mathbf{p}})$ where $\hat{\mathbf{p}}$ is a unit vector pointing in the direction of the orientation. The direct *T* matrix can be written as

$$T_{fi}^{\mathrm{dir}}(\hat{\mathbf{p}}) = \langle \Phi_f | W | \Phi_i(\hat{\mathbf{p}}) \rangle, \tag{1}$$

---
*Present address: Departamento de Fisica, Universidade Federal de Juiz de Fora, Juiz de Fora, MG 36036-330, Brazil.

where Φ_i and Φ_f are the initial- and final-state wave functions, respectively, and W is the perturbation. In the 3DW approximation, the initial-state wave function Φ_i is approximated as a product of the initial bound state of the atom $[\Psi_A(\hat{\mathbf{p}})]$ times a distorted wave function χ_i for the incoming electron (the projectile),

$$\Phi_i(\hat{\mathbf{p}}) = \Psi_A(\hat{\mathbf{p}})\chi_i. \quad (2)$$

We use numerical Hartree-Fock wave functions for the ground-state $3s$ orbital and the excited-state $3p$ orbital. The perturbation (W) is given by

$$W = V - U_i. \quad (3)$$

Here V is the interaction between the incident electron and the atom, and U_i is the initial-state spherically symmetric static approximation for V, which is asymptotically equal to zero.

The final-state wave function Φ_f is approximated as a product of two final-state continuum-electron distorted waves (χ_{scat} and χ_{eject}), and the Coulomb interaction between the outgoing electrons ($C_{\mathrm{ele-ele}}$), normally called the postcollision interaction (PCI),

$$\Phi_f = \chi_{\mathrm{scat}}\chi_{\mathrm{eject}}C_{\mathrm{ele-ele}}. \quad (4)$$

We use the exact postcollision Coulomb interaction between the two electrons ($C_{\mathrm{ele-ele}}$), which is equal to a Gamow factor times a hypergeometric function,

$$C_{\mathrm{ele-ele}} = e^{\frac{-\pi\gamma}{2}}\,\Gamma(1-i\gamma)\,{}_1F_1(i\gamma,1,-i(k_{ab}r_{ab}+\mathbf{k}_{ab}\cdot\mathbf{r}_{ab})). \quad (5)$$

Here ${}_1F_1$ is a confluent hypergeometric function, $\Gamma(1-i\gamma)$ is the gamma function, $\mathbf{k}_{ab} = \mu\,\boldsymbol{v}_{ab}$, $\mu = \frac{1}{2}$ is the reduced mass for two electrons, $\boldsymbol{v}_{ab}$ is the relative velocity between the two electrons, and γ is the Sommerfeld parameter $\gamma = \frac{1}{v_{ab}}$ which is a measure of the strength of the Coulomb interaction between the two electrons.

We would note that the 3DW approximation contains much more physics than other elementary first-order approximations such as the FBA (first Born approximation) because any "physics" contained in the initial- and final-state wave functions is automatically contained to all orders of perturbation theory. The 3DW has been remarkably successful in predicting low-energy cross sections for electron-molecule scattering recently, and we believe that the primary reason for this is the Coulomb distortion factor of Eq. (5) included in the final-state wave function. By including the Coulomb electron-electron repulsion in the final state, we are including this physics to all orders of perturbation theory. The SBA (second Born approximation), on the other hand, would just contain this effect to second order which might not be sufficient. Likewise, the distorted waves contain the interaction of the incoming projectile electron with the nucleus as well as the interaction with a spherically symmetric charge-cloud distribution to all orders, which is not contained at all in the FBA.

With these approximations, the 3DW direct T matrix becomes

$$T_{fi}^{\mathrm{dir}}(\hat{\mathbf{p}}) = \langle\chi_{\mathrm{scat}}\,\chi_{\mathrm{eject}}\,C_{\mathrm{ele-ele}}|V-U_i|\Psi_A(\hat{\mathbf{p}})\,\chi_i\rangle. \quad (6)$$

We are treating this problem as a three-body problem (one active electron in the target) so Eq. (6) is a six-dimensional

(6D) integral which we evaluate numerically. The exchange T matrix $T_{fi}^{\mathrm{exc}}(\hat{\mathbf{p}})$ is similar to Eq. (6) except that the two final-state electrons are interchanged in the final-state wave function Φ_f. Finally, the triple differential cross section (TDCS) for a fixed orientation ($\hat{\mathbf{p}}$) can be written in atomic units as

$$\frac{d^3\sigma}{d\Omega_f d\Omega_e dE_e}(\hat{\mathbf{p}}) = \frac{1}{(2\pi)^5}\frac{k_f k_e}{k_i}\big[\big|T_{fi}^{\mathrm{dir}}(\hat{\mathbf{p}})\big|^2 + \big|T_{fi}^{\mathrm{exc}}(\hat{\mathbf{p}})\big|^2$$
$$+ \big|T_{fi}^{\mathrm{dir}}(\hat{\mathbf{p}}) - T_{fi}^{\mathrm{exc}}(\hat{\mathbf{p}})\big|^2\big]. \quad (7)$$

Following Stauffer [13], the oriented wave functions $\Psi_A(\hat{\mathbf{p}})$ can be obtained by rotating the wave functions quantized with the z axis parallel to the incident beam direction. We first assume that the m-dependent wave function in the beam direction reference frame can be written as $R_{nL}(r)\,Y_{Lm}(\hat{\mathbf{r}})$ where $R_{nL}(r)$ is the radial part and $Y_{Lm}(\hat{\mathbf{r}})$ is the angular part. The charge cloud aligned by the laser beam will be an $m = 0$ state orientated parallel to the linear polarization.

Let us start with the second measurement [12]. For this case, the atom is orientated in various directions in the scattering plane. The coordinate system we use has the z axis parallel to the beam direction, the scattering plane is the xz plane, and the y axis is perpendicular to the scattering plane. Consequently, rotating the quantization axis to various directions in the scattering plane can be accomplished by rotating an angle β about the y axis. Using the rotation matrices from Rose [18] [Eq. (4.28a), p. 60], the rotated wave function in the scattering plane (SP) can be written as

$$\Psi_A(\mathrm{SP}) = \frac{\sin(\beta)}{\sqrt{2}}R_{3p}(r)[-Y_{11}(\hat{\mathbf{r}}) + Y_{1-1}(\hat{\mathbf{r}})]$$
$$+ \cos(\beta)R_{3p}(r)Y_{10}(\hat{\mathbf{r}})$$
$$= R_{3p}(r)\sqrt{\frac{3}{4\pi}}[\sin(\beta)\sin(\theta)\cos(\phi) + \cos(\beta)\cos(\theta)], \quad (8)$$

where (θ,ϕ) are the spherical angles in the beam direction reference frame. For the first measurement [11], three different orientations were measured—orientated along the x axis, the y axis, and at 45° between the x and y axes. The wave function for the x axis can be determined from Eq. (8) by setting $\beta = 90°$. For the other two cases, one must use at least two Euler angles. There are different sets of Euler angles that can be used, but the easiest set for the y axis is $(\alpha,\beta,\gamma) = (90,90,0)$. For this combination, the rotated wave function is given by

$$\Psi_A(y) = R_{3p}(r)\frac{i}{\sqrt{2}}(Y_{11} + Y_{1-1})$$
$$= R_{3p}(r)\sqrt{\frac{3}{4\pi}}\sin(\theta)\sin(\phi). \quad (9)$$

Finally, for an orientation at 45° between the x and y axes, the Euler angles are $(\alpha,\beta,\gamma) = (45,90,0)$ and the rotated wave function is given by

$$\Psi_A(xy) = R_{3p}(r)\frac{1}{2}[(-Y_{11} + Y_{1-1}) + i(Y_{11} + Y_{1-1})]$$
$$= R_{3p}(r)\sqrt{\frac{3}{8\pi}}\sin(\theta)[\cos(\phi) + \sin(\phi)]. \quad (10)$$

Consequently, one way to calculate the results for different orientations is to use Eqs. (8)–(10) to calculate the orientated wave function, and use this orientated wave function in the direct and exchange T matrices.

Alternatively, one could simply use T matrices calculated in the initial beam reference frame. For example, the spherical harmonics in Eq. (8) are expressed in the coordinate system with the z axis along the beam direction. Consequently, with substitution of the wave function (top line) of Eq. (8) into the T matrix, we obtain

$$T_{fi}(\text{SP}) = \frac{\sin(\beta)}{\sqrt{2}} \left[-\Upsilon_1 + \Upsilon_{-1} \right] + \cos(\beta)\Upsilon_0. \quad (11)$$

where Υ_m is the T matrix for a coordinate system with the z axis parallel to the beam direction. This is Eq. (4) of Stauffer [13] for the case $\varepsilon = -\beta$ (to compare with experiment, we will use $-\beta$ in the calculations). It is well known that, for this atomic system, $\Upsilon_1 = -\Upsilon_{-1}$ from symmetry so that

$$T_{fi}(\text{SP}) = -\sqrt{2}\sin(\beta)\Upsilon_1 + \cos(\beta)\Upsilon_0. \quad (12)$$

For the x-axis orientation we have Eq. (12) with $\beta = 90°$,

$$T_{fi}(x) = -\sqrt{2}\Upsilon_1. \quad (13)$$

For the y axis, Eq. (9) yields

$$T_{fi}(y) = \frac{i}{\sqrt{2}} \left(\Upsilon_1 + \Upsilon_{-1} \right). \quad (14)$$

Now, symmetry about the scattering plane ($\Upsilon_{-1} = -\Upsilon_1$) reduces this expression to

$$T_{fi}(y) = 0. \quad (15)$$

And finally for the xy orientation, Eq. (10) gives us

$$T_{fi}(xy) = \tfrac{1}{2}[(-1+i)\Upsilon_1 + (1+i)\Upsilon_{-1}] = -\Upsilon_1. \quad (16)$$

Consequently, for orientations in the perpendicular plane, we conclude that the cross sections for the y-axis orientation should be zero and the x-axis orientation should have cross sections twice as large as those for the xy orientation, since the cross sections are proportional to the absolute value of the T matrix squared.

From Eqs. (12), (13), (15), and (16), we see that the cross sections for any orientation can be calculated from the Υ_0 and Υ_1 amplitudes as was pointed out by Stauffer [13]. More explicitly, we have both direct and exchange amplitudes so we use Eqs. (12), (13), and (16) for both the direct and exchange T matrices. Consequently, for the scattering plane (SP) we would have

$$T_{fi}^{\text{dir}}(\text{SP}) = -\sqrt{2}\sin(\beta)\Upsilon_1^{\text{dir}} + \cos(\beta)\Upsilon_0^{\text{dir}}, \quad (17)$$

and

$$T_{fi}^{\text{exc}}(\text{SP}) = -\sqrt{2}\sin(\beta)\Upsilon_1^{\text{exc}} + \cos(\beta)\Upsilon_0^{\text{exc}}, \quad (18)$$

and then use Eq. (7) to calculate cross sections. Typically the exchange amplitude is ignored, which is the case considered by Eq. (5) of Stauffer [13]. Since Eqs. (17) and (18) have the same form of dependence on the orientation angle β, a linear combination of these amplitudes will also have this form. Moreover, a linear combination of the squared moduli of these

amplitudes as in Eq. (7) will have the same dependence on the orientation angle as given in Eq. (5) of [13]. We have verified that we obtain the same cross sections using the wave function of Eq. (8) to calculate the T matrix for the rotated wave function and the amplitudes of Eqs. (17) and (18) calculated in the nonrotated reference frame.

III. RESULTS AND DISCUSSION

Triple differential cross sections (TDCSs) for ionization of the (3*s*) ground state are presented in Fig. 1 for equal final-state energies and asymmetric angles. The figure contains a comparison of 3DW, distorted wave Born approximation (DWBA), and TDCC results with the measurements of Nixon and Murray [11]. DWBA results are calculated in the same manner as the 3DW except that the Coulomb interaction factor ($C_{\text{ele-ele}}$) in Eq. (4) is set equal to unity. Consequently the 3DW results have the postcollision interaction (PCI) contained to all orders of perturbation theory, while the DWBA contains this interaction only to first order. Since the experiments are not absolute, all the theories and the experimental data are normalized to unity at the binary peak. It is seen that the 3DW results are in excellent agreement with the measurements for an initial 3*s* state. Both the DWBA and TDCC predict binary peaks shifted to smaller angles and these calculations display a similar trend over the full range of electron ejection angles.
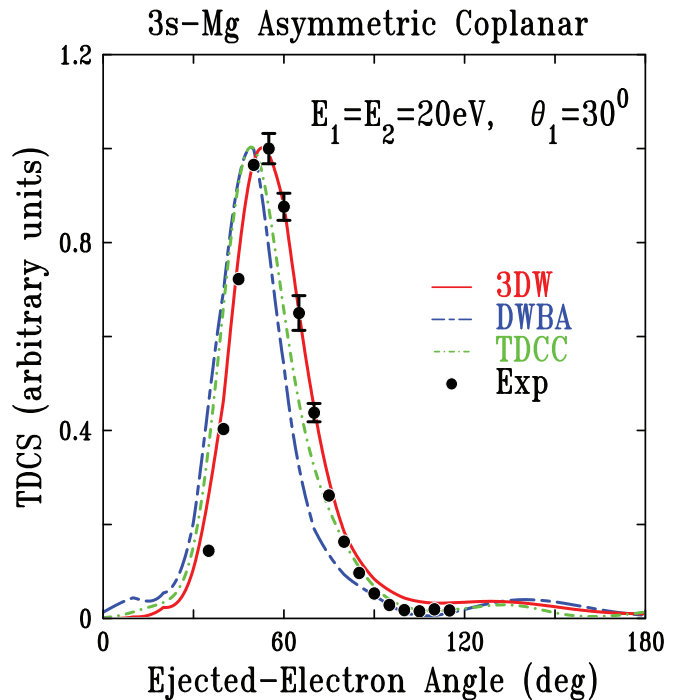

FIG. 1. (Color online) Experimental and theoretical TDCS for electron-impact ionization of the 3*s* state of Mg. The projectile scattering angle θ_1 is 30° and both outgoing electrons have the same energy ($E_1 = E_2 = 20$ eV). The theoretical calculations are 3DW: solid red; DWBA: dashed blue; and TDCC: dash-dot green. The experimental data are the solid circles. See text for normalization of theories and experiment.
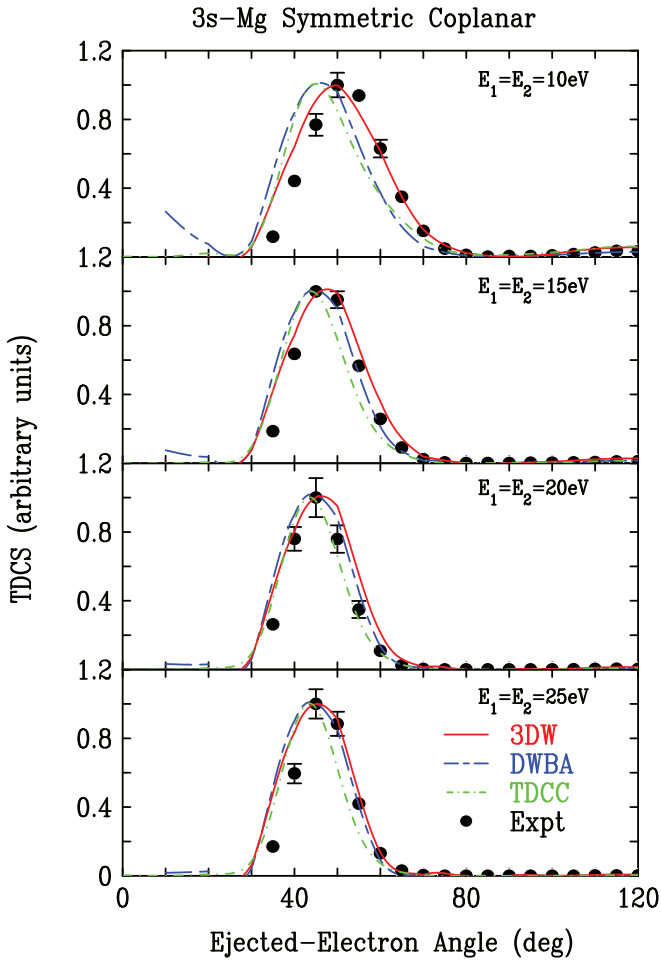
FIG. 2. (Color online) Experimental and theoretical TDCS for electron-impact ionization of the 3*s* state of Mg for symmetric coplanar geometry. The energies for outgoing electrons are equal and vary for the four panels ranging from 10 to 25 eV. The theoretical calculations are 3DW: solid red; DWBA: dashed blue; and TDCC: dash-dot green. The experimental data are the solid circles. See text for normalization of theories and experiment.

Figure 2 shows 3DW, DWBA, and TDCC results compared with experiment for Mg (3*s*) coplanar symmetric angles and energies. The different panels are for different final-state electron energies starting from 10 eV at the top to 25 eV at the bottom. In general, all three theories are in reasonably good agreement with the experimental data. For most of the cases, it can be seen that the 3DW exhibits a little better agreement with experimental data than the other two theories. Both the DWBA and TDCC are becoming in better agreement as the outgoing electrons energy increases from 10 to 25 eV.

In Fig. 3, we present triple differential cross sections for magnesium atoms laser aligned in a plane perpendicular to the incident electron beam and parallel to the linear polarization. We use a coordinate system for which the incident beam direction is the *z* axis, the scattering plane is the *xz* plane, and the *xy* plane is the plane perpendicular to the incident beam. For all these measurements, the incident projectile electron had an energy of 43.31 eV, the scattered and ejected electrons had equal energies ($E_1 = E_2 = 20$ eV), one of the final-state
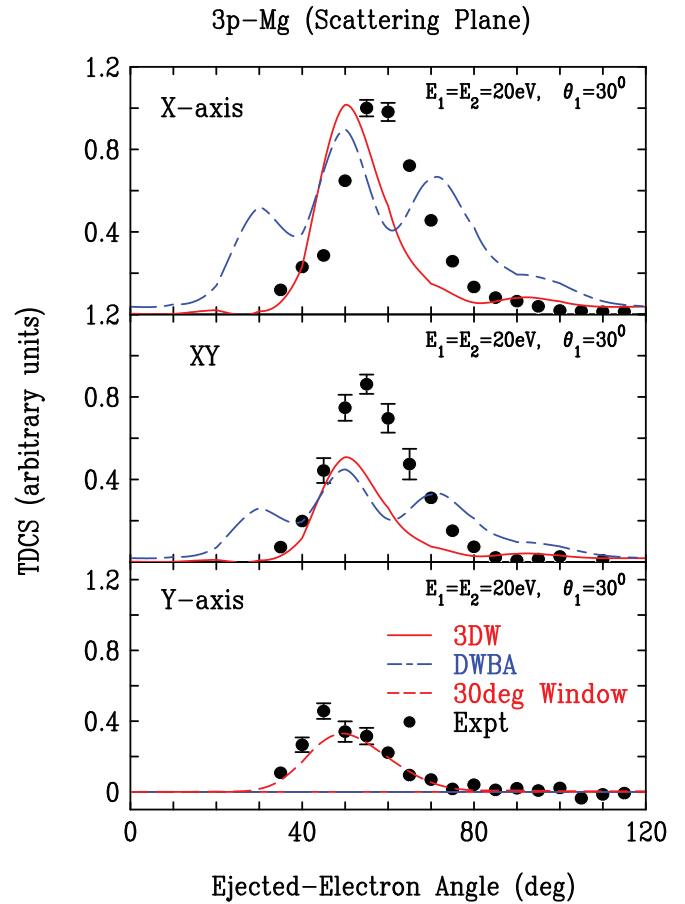

FIG. 3. (Color online) Experimental and theoretical TDCS for electron-impact ionization of the laser-aligned 3*p* state of Mg. The projectile scattering angle θ_1 is 30° and both outgoing electrons have the same energy ($E_1 = E_2 = 20$ eV). The three panels are for laser alignment parallel to the *x* axis (see text), laser alignment at 45° between the *x* and *y* axes, and laser alignment parallel to the *y* axis, respectively. In the bottom panel, the 3DW and DWBA results are exactly zero. The theoretical calculations are 3DW: solid red; DWBA: dash-dot blue; and (30° window) dashed red are the 3DW results convoluted over an angular uncertainty of ±30°. The experimental data are the solid circles. See text for normalization of theories and experiment.

electrons was detected at a fixed scattering angle of 30°, and the other final-state electron was detected at angles ranging between 35° and 120°. The upper panel corresponds to an alignment parallel to the *x* axis, the middle panel corresponds to an alignment at 45° between the *x* and *y* axes, and the lower panel is for ionization of the 3*p* state that has been laser aligned parallel to the *y* axis (perpendicular to the incident beam and perpendicular to the scattering plane). We have normalized the experiment and 3DW to unity at the maximum cross section for the *x* axes (upper panel). We use the same normalization factor for the DWBA as the 3DW. The experimental data for the excited states are relatively absolute (i.e., they have been internormalized by measuring the cross sections at $\theta_2 = 50°$ for the various laser orientations), so the same normalization is used for Figs. 3–5. In the upper panel, it is seen that the 3DW predicts the proper shape of the cross section but the
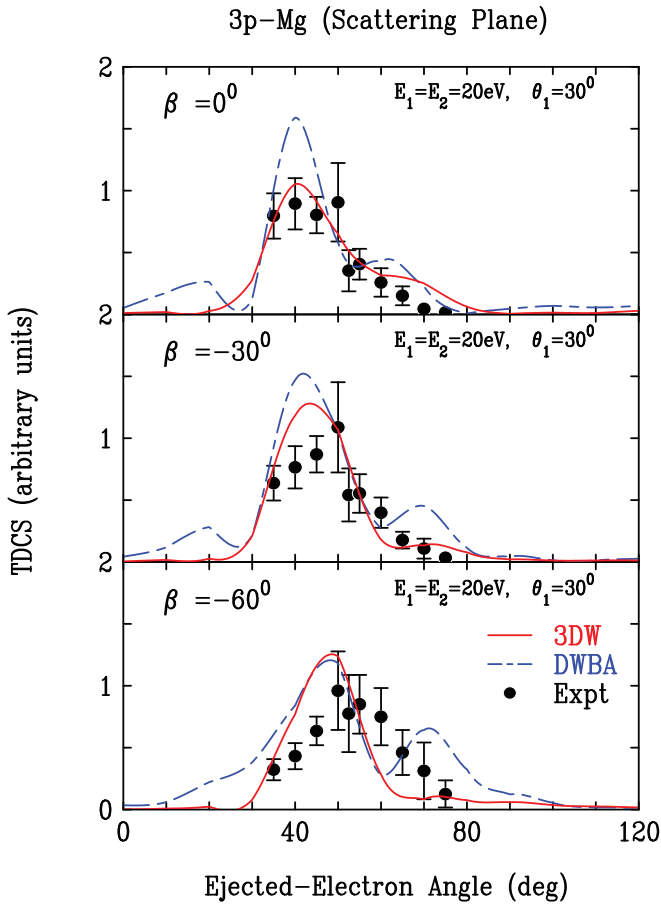
FIG. 4. (Color online) Experimental and theoretical TDCS for electron-impact ionization of the laser-aligned 3p state of Mg. The projectile scattering angle θ_1 is 30° and both outgoing electrons have the same energy ($E_1 = E_2 = 20\,\mathrm{eV}$). The three panels are for laser alignment in the scattering plane by different orientation angles "beta" relative to the incident beam direction. The theoretical calculations are 3DW: solid red; DWBA: dash-dot blue; the experimental data are the solid circles. See text for normalization of theories and experiment.

FIG. 5. (Color online) Same as in Fig. 4.

experimental peak is shifted to lower angles. The DWBA has the wrong shape with three peaks instead of one. The fact that the 3DW has the correct shape while the DWBA does not indicates that the Coulomb interaction between the two electrons (PCI) plays a major role in this collision. Looking at the middle panel (alignment at 45° between the x and y axes), the DWBA and 3DW results are exactly half the results in the upper panel, as was expected from Eqs. (13) and (16). However, the results shown in the figure were obtained using the orientated wave functions of Eqs. (8) and (10). Obviously, the experimental data are not in accord with the symmetry prediction.

Experimental results for ionization of a 3p state that has been laser aligned parallel to the y axis are shown in the lower panel in Fig. 3. For this case the 3DW and DWBA numerical results were exactly zero using the orientated wave function of Eq. (9) for all ejected electron angles in accordance with the prediction of Eq. (15). Since the experiment finds significant nonzero results for this orientation, we thought that the problem might be with angular resolution of the
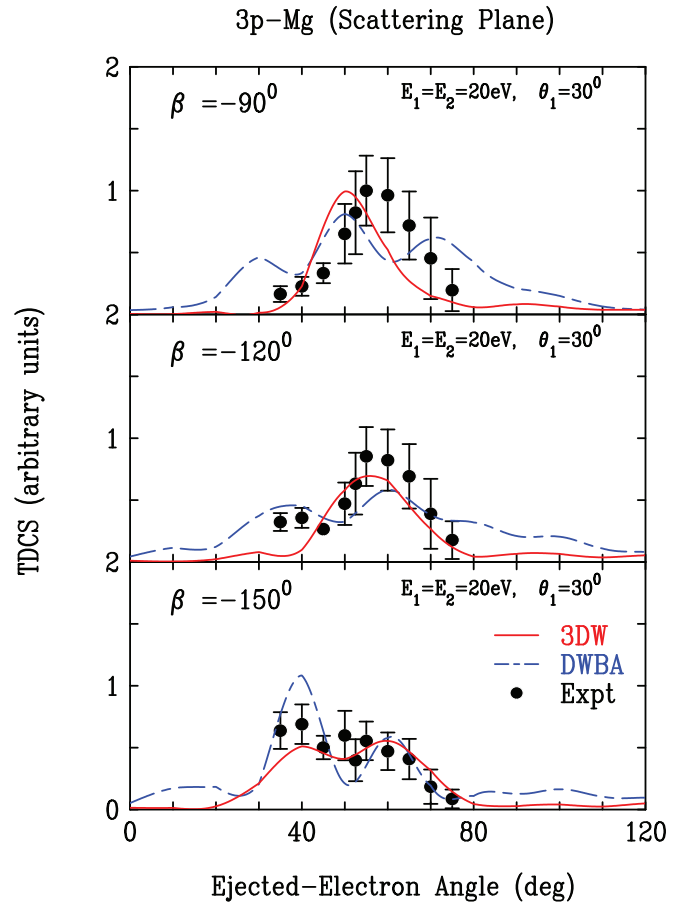
experiment. The experimental acceptance angular range is ±3° so we convoluted our theoretical results over this angular range. While we then found a small nonzero cross section, it was still much smaller than experiment. As an interesting exercise, we tried making the acceptance window wider and found that ±30° yielded excellent agreement with experiment (dashed red in bottom panel). Obviously this is much larger than the experiment measures, and we show the results for academic interest only.

In Figs. 4 and 5, we show results for ionization of a 3p state that has been laser aligned to different orientation angles β ranging from 0° to −150° in the scattering plane (0° means the incident beam direction, and a negative angle means clockwise rotation). Figure 4 shows results for three different β (0°, −30°, and −60°). The 3DW results are in reasonably good agreement with the experimental data for most cases. However, the peak in the experimental data shifts a few degrees to the right as the orientation angle (β) increases (see Fig. 4). However, overall the 3DW shows much better agreement with experimental data than the DWBA, which has a three-peak structure not seen in the data.

Figure 5 shows the comparison between theory and experiment for the same kinematics as Fig. 4 but for higher orientation angles (−90°, −120°, and −150°). Although the upper panel for $\beta = -90°$ corresponds to the x axis results for Fig. 3, this is a different data set taken at a different time.

As mentioned earlier, this is the case we used for normalizing both the theory and experiment. Comparing the *x*-axis results for Figs. 3 and 5, it is seen that the experimental data are in agreement with each other, and the comparison with theory looks the same in both cases. In both the middle and the lower panel, the 3DW still predicts most of the experimental data with the location of the experimental peak becoming closer to the data as well. Interestingly, the DWBA showed much better agreement with the experimental data in the middle panel as well as the lower one.

IV. ANALYSIS OF THE EXPERIMENTAL DATA

A. Effects of depolarization on the experimental data

The large difference found between theory and experiment when the electron charge-cloud alignment is positioned out of the scattering plane requires further consideration. This discrepancy is particularly significant when the state is aligned orthogonal to the plane, since as shown here the calculations predict a zero in the ionization cross section due to symmetry, which the experiments do not find. Indeed as is shown earlier in this paper, for theory to emulate the data under these conditions, the acceptance angles of the electron analyzers would need to be ∼10 times larger than they are. It is therefore sensible to investigate whether other experimental artifacts may be playing a role in this discrepancy.

One difference between experiment and theory is that the calculation assumes the *P* state is a pure $3\,^1P_1$ state that is fully aligned orthogonal to the scattering plane by the laser beam. In practice this is not possible, since the laser will have a small elliptically polarized component, with the major axis of this ellipse being orthogonal to the plane. In this case the atoms will be excited with a small state amplitude in the scattering plane that depends upon the degree of ellipticity, due to the electric field component of the light that lies along the minor axis of the ellipse.

A second effect that may play a role is that of radiation trapping in the interaction region. Radiation trapping can occur when the incident laser radiation couples to atoms in the ground state [19], as in the experiments described here. In this case, radiation emitted from a laser-excited atom that decays back to the ground state may be reabsorbed by a second atom that is in the ground state. This second excited atom will then spontaneously emit a photon, whose direction and polarization are uncorrelated with the laser field. Further absorption and reemission processes may then occur, so that the radiation is effectively "trapped" inside the interaction region for several decay cycles. The probability of this occurring depends upon the density of atoms in the interaction region, the trapping cycle leading to an overall depolarization of the light emitted from the ensemble. If the trapping process is significant, this would also produce a relative population of excited atoms whose alignment is in the scattering plane.

To establish the degree of importance of these processes, measurements were made of the fluorescence emitted from the atomic ensemble using a silicon carbide photodiode that was sensitive to the emitted light at a wavelength of ∼285 nm. The radiation was collected using a 50-mm-diameter fused silica lens that imaged the interaction region onto the photodiode.

The axis of detection was orthogonal to the incident laser and electron beams, and was in the scattering plane [11,12].

The normal way to determine the significance of the effects discussed above is to measure the polarization of fluorescence from a pure state (such as the $3\,^1P_1$ state in Mg used here), since this should be ∼100% for a fully aligned atom with no trapping in the interaction region. This technique was not possible in the current experiments, as efficient linear dichroic polarizers do not exist for radiation at 285 nm. The polarizer that set the laser polarization was a Barium Borate (BBO) Glan-laser polarizer that does have high efficiency at this wavelength; however, this type of polarizer cannot be used when detecting fluorescence. In the experiments [11,12] the angle of the incident laser polarization vector was adjusted using a zero-order half-wave plate that was positioned in the beam path after the BBO polarizer, and it is this that could introduce a small ellipticity to the incident laser beam.

To establish if the effects of trapping and/or polarization change were significant, the angle of polarization of the incoming laser was varied, and the change in intensity on the photodiode was monitored. For a laser polarization vector orthogonal to the direction of detection, a maximum intensity is expected (since observations are side-on to the excited *P* state). When the polarization vector points in the direction of detection, a minimum in the fluorescence should then occur (all radiation from a pure state then being emitted in other directions). For a fully aligned *P* state the minimum intensity $I_\perp$ should hence be very close to zero. In this case a fluorescence polarization can be defined, and for a pure *P* state this is given by

$$P_1^{\text{Fluor}} = \frac{I_\parallel - I_\perp}{I_\parallel + I_\perp} \sim 1. \qquad (19)$$

If $P_1^{\text{Fluor}} < 1$ this is evidence of either radiation trapping or that the incoming laser beam is elliptically polarized (it is not possible to distinguish between these different processes from this parameter).

Measurements in the experiments using this technique produced a fluorescence polarization $P_1^{\text{Fluor}} = 0.95 \pm 0.03$, as shown in Fig. 6. Although this is close to unity, it does indicate a small effect may be occurring due to radiation
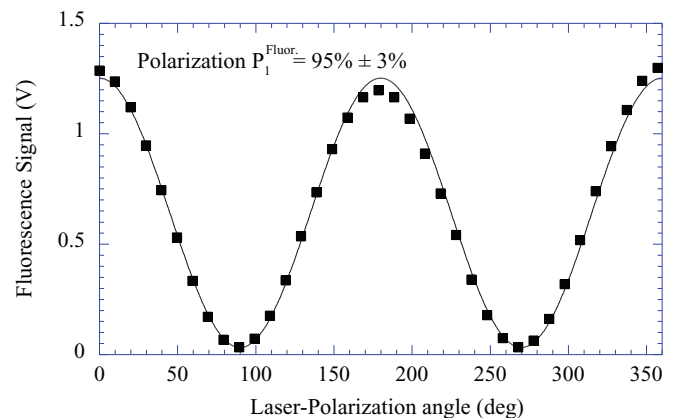
FIG. 6. (Color online) Variation of the measured fluorescence signal as a function of the polarization angle of the laser beam.

trapping, or due to a slight elliptical polarization of the laser beam. There will also be a small contribution due to the finite acceptance angle of the collecting lens, which also reduces the polarization. In the present discussion the effects of the collecting lens are ignored, allowing an upper bound to be placed on the relative population of excited targets aligned in the scattering plane due to trapping or ellipticity of the laser beam.

B. In-plane excited-state population estimates due to radiation trapping

If the depolarization shown in Fig. 6 is all due to radiation trapping, an estimate of the relative population of excited targets in the scattering plane can be made. Due to the random nature of the spontaneous emission process, the trapped radiation can be considered as having equal intensity I^{Tr} in all directions. In this case the fluorescence polarization due to radiation trapping will be given by

$$P_1^{\text{RT}} = 0.95 = \frac{(I_\parallel^{\text{NT}} + I^{\text{Tr}}) - I^{\text{Tr}}}{(I_\parallel^{\text{NT}} + I^{\text{Tr}}) + I^{\text{Tr}}}$$

$$= \frac{I_\parallel^{\text{NT}}}{I_\parallel^{\text{NT}} + 2I^{\text{Tr}}} \Rightarrow I_\parallel^{\text{NT}} = 38I^{\text{Tr}}, \quad (20)$$

where $I_\parallel^{\text{NT}}$ is the intensity with no radiation trapping present. Hence ~2.6% of the light is emitted in each orthogonal direction due to radiation trapping. As one of these directions is not observed in the experiment (that is, where the emitting dipoles lie in the scattering plane, and point along the direction of observation), there are then two contributions that can produce excited atoms in the scattering plane, and so at most ~5.2% of the atoms will be aligned in this plane. From these experimental data, radiation trapping can hence only make a small contribution to the measured ionization cross section.

C. In-plane excited-state population due to residual ellipticity of the laser beam polarization

The second process that can lead to $P_1^{\text{Fluor}} < 1$ is due to the incident laser beam being *elliptically* polarized rather than linearly polarized, as noted above. In this case the excited target is once again a pure $3\,^1P_1$ state; however, the transition from the ground $3\,^1S_0$ state will no longer obey the selection rule $\Delta m_J = 0$ for a quantization axis chosen along the direction of the polarization vector.

Under these conditions it is sensible to adopt a quantization axis along the laser beam direction [20]. In this configuration linearly polarized radiation excites both $|J,m_J\rangle = |1,\pm1\rangle$ states with equal amplitude, the normalized wave function then being represented as

$$|\psi\rangle^{3\,^1P_1} = a_{+1}|1,+1\rangle + a_{-1}|1,+1\rangle$$

$$= \frac{1}{\sqrt{2}}(e^{i\varepsilon}|1,+1\rangle + e^{-i\varepsilon}|1,-1\rangle), \quad (21)$$

where ε is a phase angle that defines the direction of polarization. A similar approach can also be formulated to describe an atom excited by *elliptically* polarized radiation. In this case the substate amplitudes $a_{\pm1}$ will be unequal in magnitude, and the phase angle ε then defines the direction of the major axis of the charge cloud.

It is easiest to adopt a density matrix formalism to describe the resulting P state, since the density matrix in this frame ρ^{Las} can then be rotated into the reference frame of the detector [20]. The relative fluorescence ratio $I_\parallel / I_\perp$ can then be calculated by an appropriate choice of rotation operators acting on ρ^{Las}.

For a fluorescence polarization P_1^{Fluor} as measured above, the density matrix ρ^{Las} for elliptically polarized excitation is
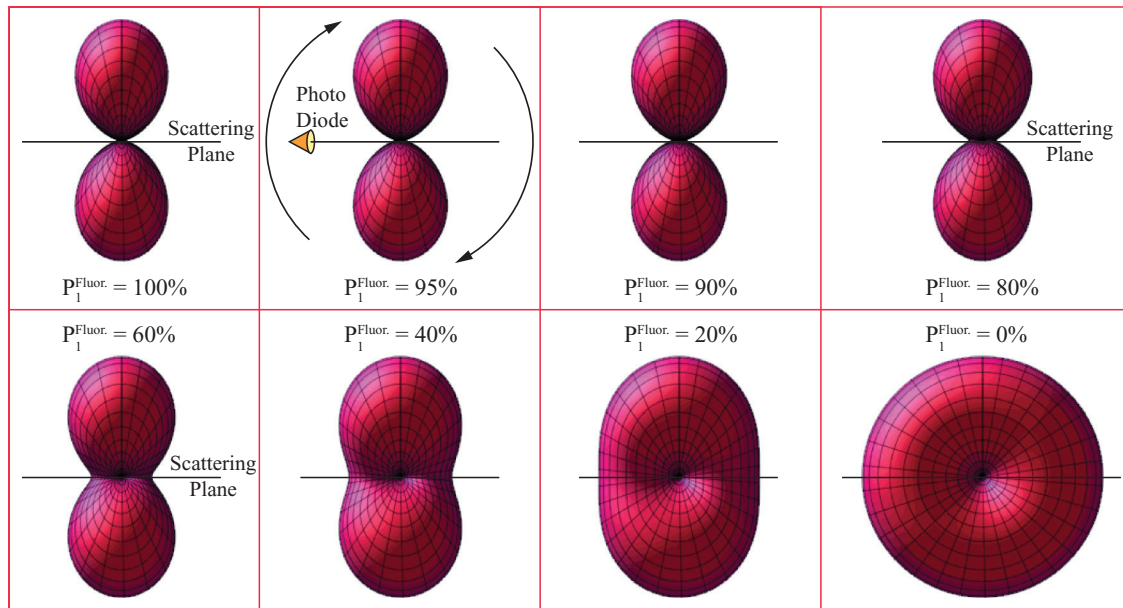

FIG. 7. (Color online) Examples of the angular shape of the pure *P*-state charge cloud excited by elliptically polarized laser radiation that produces different values of the fluorescence polarization. The arrows show how the state is rotated with respect to the detector so as to measure P_1^{Fluor}.

then calculated to be

$$
\rho_{ij}^{\text{Las}} = \frac{1}{2}
\begin{bmatrix}
1 \pm \sqrt{1 - \left(P_1^{\text{Fluor}}\right)^2} & 0 & -P_1^{\text{Fluor}}\exp(-2i\varepsilon) \\
0 & 0 & 0 \\
-P_1^{\text{Fluor}}\exp(+2i\varepsilon) & 0 & 1 \mp \sqrt{1 - \left(P_1^{\text{Fluor}}\right)^2}
\end{bmatrix},
$$

(22)

where ε defines the direction of the major axis of the charge cloud with respect to the scattering plane, and the sign of the terms in ρ_{11} and ρ_{-1-1} are set by the handedness of the radiation. Under the conditions for a charge cloud that has a major axis orthogonal to the scattering plane, the relative population of atoms in the scattering plane is found to be directly related to $I_\parallel / I_\perp$. Hence for $P_1^{\text{Fluor}} = 0.95$, the major axis of the charge cloud orthogonal to the scattering plane is $\sim$39 times larger than the minor axis that lies in the plane. Figure 7 shows examples of the charge-cloud angular "shape" that would produce different values of P_1^{Fluor}, where the charge cloud is viewed from the direction of the photodiode for vertical alignment of the cloud (i.e., out of the scattering plane). For a fluorescence polarization of 95%, the contribution from the ellipticity of the laser light is hence expected to only make a small change to the measured ionization cross section, since as seen in Fig. 7, the in-plane contribution only becomes substantial when the polarization reduces below $\sim$80%.

V. CONCLUSION

In conclusion, we have compared experiment and theory for electron-impact ionization of the ground state of Mg as well as ionization of a $3p$ state that has been laser aligned either in the scattering plane or in a plane perpendicular to the incident beam direction. For the ground-state ionization, the experimental results were compared with TDCC (time-dependent close coupling), DWBA (distorted wave Born approximation), and 3DW (three-body distorted wave) approximations. While all three theoretical approaches gave reasonably good agreement with the data, the 3DW predicts the location of the binary peak and width a little better.

For ionization of the laser-aligned $3p$ state, the experiment was compared with DWBA and 3DW calculations. The experimental data are relatively absolute, so only one normalization places all the data on an absolute scale. We chose to normalize to the measurement with the alignment parallel to the x axis, since this was the common alignment direction in the two different data sets. For alignment in the scattering plane, the 3DW results were in very good agreement with experiment with the only problem being a small shift in peak location for $\beta = (-30°, -60°, -90°)$. For larger and smaller β, the 3DW peak locations are in agreement with experiment. Since all the different orientations can be calculated from the $m = (0,1)$ amplitudes calculated relative to the z axis being parallel to the incident beam direction, this comparison is an indirect test of the accuracy of the Υ_m amplitudes for $m = (0,1)$.

For the beam direction along the z axis, we have the well-known symmetry $\Upsilon_{-1} = -\Upsilon_1$. For the case of ionization of the $3p$ state with alignment angles in the perpendicular plane, this symmetry predicts that the cross sections for alignment at 45° between the x and y axes should be half the cross sections for the x-axis alignment, and the cross sections for alignment along the y axis should be zero. Although the theoretical cross sections satisfied these conditions, the experimental data did not. On the other hand, we have learned from the experimental approach and its analysis of the polarization data mentioned above that the effects of both radiation trapping and an elliptically polarized laser beam will not substantially alter the experimental results. In both cases the relative change is found to be 5% or less. This cannot explain the large discrepancy between theory and experiment that is found when the excited state is aligned orthogonal to the scattering plane. The angular acceptance of the detectors has also been discounted as a significant contributing factor. At the present time it is hence difficult to see where this discrepancy originates, and the results in this paper clearly show that more work is needed to resolve the cause of these differences.

[1] A. Senftleben, T. Pflueger, X. Ren, O. Al-Hagan, B. Najjari, D. Madison, A. Dorn, and J. Ullrich, J. Phys. B **43**, 081002 (2010).

[2] A. Senftleben, O. Al-Hagan, T. Pflueger, X. Ren, D. Madison, A. Dorn, and J. Ullrich, J. Chem. Phys. **133**, 044302 (2010).

[3] X. Ren, T. Pfluger, S. Xu, A. Senftleben, J. Colgan, M. S. Pindzola, A. Dorn, and J. Ullrich, J. Phys.: Conf. Ser. **388**, 052037 (2012).

[4] J. C. A. Lower, E. Ali, S. Bellm, E. Weigold, A. Harris, C. G. Ning, and D. Madison, Phys. Rev. A **88**, 062705 (2013).

[5] E. Ali, A. L. Harris, J. Lower, E. Weigold, C. G. Ning, and D. H. Madison, Phys. Rev. A **89**, 062713 (2014).

[6] J. Gao, J. L. Peacher, and D. H. Madison, J. Chem. Phys. **123**, 204302 (2005).

[7] J. Colgan, M. S. Pindzola, F. Robicheaux, C. Kaiser, A. J. Murray, and D. H. Madison, Phys. Rev. Lett. **101**, 233201 (2008).

[8] E. M. Staicu Cassagrande, A. Naja, F. Mezdari, A. Lahmam-Bennani, P. Bolognesi, B. Joulakian, O. Chuluunbaatar, O. Al-Hagan, D. H. Madison, D. V. Fursa, and I. Bray, J. Phys. B **41**, 025204 (2008).

[9] O. Al-Hagan, C. Kaiser, D. H. Madison, and A. J. Murray, Nat. Phys. **5**, 59 (2009).

[10] A. J. Murray, J. Phys.: Conf. Ser. **212**, 012016 (2010).

[11] K. L. Nixon and A. J. Murray, Phys. Rev. Lett. **106**, 123201 (2011).

[12] K. L. Nixon and A. J. Murray, Phys. Rev. Lett. **112**, 023202 (2014).

[13] A. D. Stauffer, Phys. Rev. A **89**, 032710 (2014); **89**, 049906(E) (2014).

[14] G. S. J. Armstrong, J. Colgan, and M. S. Pindzola, Phys. Rev. A **88**, 042713 (2013).

[15] J. Colgan and M. S. Pindzola, Eur. Phys. J. D **66**, 284 (2012).

[16] D. H. Madison and O. Al-Hagan, J. At. Mol. Opt. Phys. **2010**, 367180 (2010).

[17] S. Amami, M. Ulu, Z. N. Ozer, M. Yavuz, S. Kazgoz, M. Dogan, O. Zatsarinny, K. Bartschat, and D. Madison, Phys. Rev. A **90**, 012704 (2014).

[18] M. E. Rose, *Elementary Theory of Angular Momentum*, 5th ed. (John Wiley & Sons, New York, 1967).

[19] A. J. Murray, W. R. MacGillivray, and M. C. Standage, Phys. Rev. A **44**, 3162 (1991).

[20] A. J. Murray, W. MacGillivray, and M. Hussey, Phys. Rev. A **77**, 013409 (2008).